

# PH4103 Term Paper

## Measurement of sub-milliohm resistance of a copper wire using an SR830 Lock-in Amplifier

Debayan Sarkar

22MS002

Diptanuj Sarkar

22MS038

Sabarno Saha

22MS037

Supervisor: Prof. Kamaraju Natarajan  
Prof. Sourin Das

Date: 27 November 2025

### Abstract

In this experiment, we make use of a lock-in amplifier to measure sub-milliohm resistance of a copper wire. To do this, we set up a two-probe measurement configuration where we pass a small AC current through the copper wire and measure the resulting voltage drop across it using the lock-in amplifier. We also characterize flicker noise ( $1/f$  noise) observed in resistors and compare it with theoretical estimates. We also detail the basic working principle of a lock-in amplifier in this report.

### Contents

<b>1. The Lock-In Amplifier</b>	<b>3</b>
1.1. Introduction .....	3
1.2. Working Principle .....	3
1.3. Core Blocks and Specifications of the SR830 .....	5
1.3.1. Input and Reference Signals .....	5
1.3.2. Digital Low Pass Filters .....	5
1.3.3. Synchronous Filters .....	5
1.4. Noise Sources of the SR830 .....	5
1.4.1. Johnson Noise .....	6
1.4.2. Shot Noise .....	6
1.4.3. $1/f$ Noise .....	6
1.4.4. External Noises .....	6
<b>2. Flicker Noise</b>	<b>6</b>
2.1. $\frac{1}{f^\alpha}$ noise from the superposition of relaxation processes .....	7
2.2. Can the fluctuations be infinitely large? .....	9
<b>3. Four Terminal AC Resistance Measurement</b>	<b>9</b>
3.1. Contact resistance .....	11

---

3.2. Preparation of sample for 4-point measurement .....	11
3.3. BNC Cables .....	11
<b>4. Sub-Milliohm Resistance Measurement</b>	<b>12</b>
4.1. Procedure .....	12
4.2. Circuit Diagram .....	13
4.3. Parameters .....	13
4.4. Analysis .....	13
4.5. Resistance .....	15
4.6. Errors .....	16
4.7. Observations .....	17
4.8. Sources of Error .....	20
4.9. Conclusion .....	20
<b>5. 1/f noise analysis</b>	<b>20</b>
5.1. Working Principle .....	21
5.2. Parameters .....	21
5.3. Data analysis .....	22
5.4. Observations .....	23
<b>6. Conclusion</b>	<b>23</b>
<b>References</b>	<b>24</b>

# 1. The Lock-In Amplifier

## 1.1. Introduction

A lock-in amplifier is a type of amplifier that can extract a signal from an extremely noisy input. Generally, the signal we are trying to extract has a known carrier signal, i.e. a known frequency. The signal to noise ratio upto which we can reliably detect the target signal depends on the dynamic reserve of the instrument. For our experiments, we used Stanford Research Systems' Model SR830 DSP Lock-In Amplifier. As a DSP (Digital Signal Processor) lock-in amplifier, the SR830 performs most of it's core functions digitally, leading to a better performance than it's analog competitors. In the following section, we describe the workings of this amplifier in greater detail.

## 1.2. Working Principle

The core function that the lock-in amplifier performs, is *Phase Sensitive Detection*. Let's say the input signal we provide is  $V_i(t) = V_0 \sin(\omega_i t + \varphi_i)$ . The lock-in multiplies this signal with another reference signal, often provided by an internal oscillator. Let's say the reference sinusoidal signal is given by  $V_r(t) = V_1 \sin(\omega_r t + \varphi_r)$ . Note that both  $\omega_r$  and  $\varphi_r$  of this internal oscillator are tunable parameters. After multiplying these two signals, we get

$$\begin{aligned} V_{\text{psd}}(t) &= V_i(t)V_r(t) \\ &= V_0 V_1 \sin(\omega_i t + \varphi_i) \sin(\omega_r t + \varphi_r) \\ &= \frac{1}{2} V_0 V_1 [\cos[(\omega_i - \omega_r)t + (\varphi_i - \varphi_r)] - \cos[(\omega_i + \omega_r)t + (\varphi_i + \varphi_r)]] \end{aligned} \quad (1.1)$$

As we can see, we end up with two different sinusoidal components. If  $\omega_i = \omega_r$ , then we end up with an oscillating AC signal at frequency  $2\omega_r$  and a DC offset signal. If we now send this signal through a low pass filter (or equivalently take a time average of the signal), we will end up with just the DC signal, which from our calculations turns out to be,

$$V_{\text{lpf}} = \frac{1}{2} V_0 V_1 \cos(\Delta\varphi) \quad (1.2)$$

Where  $\Delta\varphi = \varphi_i - \varphi_r$ , can be adjusted to 0 by setting  $\varphi_r = \varphi_i$ . The output of the low pass filter can then be scaled down by  $\frac{1}{2}V_r$ , and we finally end up with the output voltage of  $V_{\text{out}} = V_0$ . Note that it's not necessary that the input signal is a pure sinusoid. Infact, most of the times it will not be one.

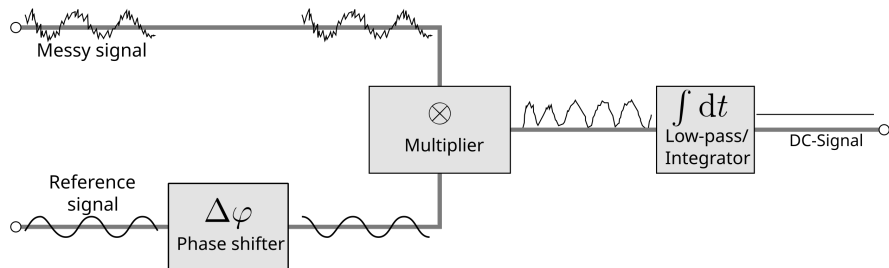


**Figure 1:** Schematic diagram of a Phase Sensitive Detector (Credits: Zelbear on Wikipedia)

We can use the lock-in amplifier to extract all the fourier components of the target signal at the reference frequency. To do this, the lock-in performs the calculation we just described, twice in the two quadratures by using a  $90^\circ$  phase shifted copy of the reference signal. It's better explained by this schematic diagram shown below.

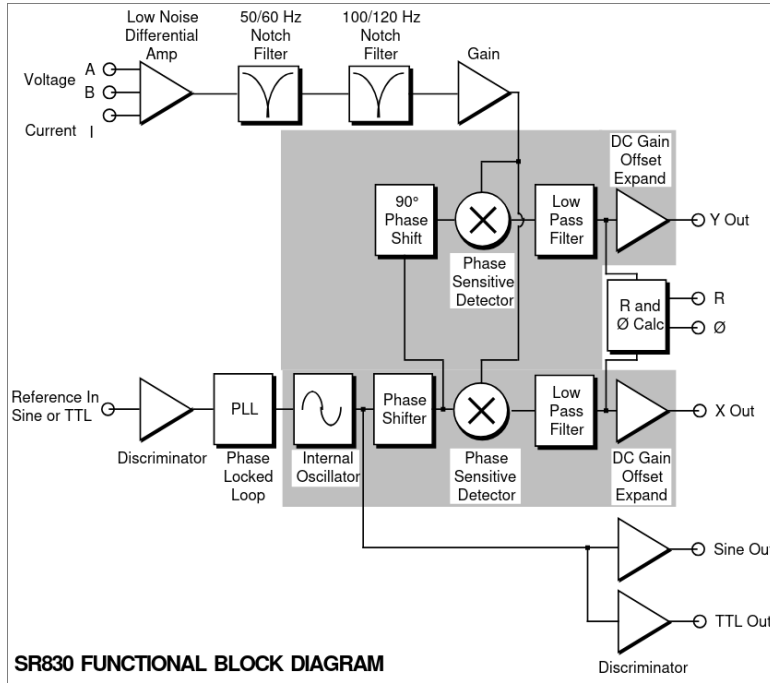


**Figure 2:** Schematic Diagram for the SR830 Lock-In Amplifier (Credits: Stanford Research Systems)

And the end of this process, we end up with two signals,  $X$  and  $Y$ , which correspond to the sin and cos quadratures of the signal respectively. The lock-in also calculates two other variables  $R$  and  $\theta$  as

$$R = \sqrt{X^2 + Y^2} \quad (1.3)$$

$$\theta = \arctan\left(\frac{Y}{X}\right) \quad (1.4)$$

## 1.3. Core Blocks and Specifications of the SR830

In this section we describe the core blocks of the SR830 lock-in amplifier, along with the various specifications and available values for the adjustable parameters in those blocks. Below is an image of the front-panel of the SR830.

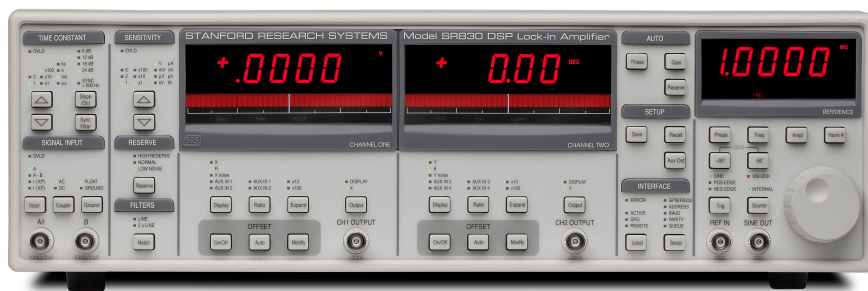


**Figure 3:** Front Panel of the SR830 (Credits: Stanford Research Systems)

As mentioned before, all the core functionalities in an SR830 are done using a DSP (Digital Signal Processor).

### 1.3.1. Input and Reference Signals

The analog input signal is digitised, into a 20 bits, 256 kHz sample-rate digital signal. After this, all the computation for phase sensitive detection that we discussed before, is done digitally using the DSP. Even the reference signal is digitally synthesized. The **SINE OUT** signal is just that digitally synthesized signal, passed through a Digital to Analog Converter. For the reference signal, we can adjust the Phase, Frequency and Amplitude.

### 1.3.2. Digital Low Pass Filters

The SR830 uses digital filters, which again are implemented using the DSP. Since the filters are digital, we are not limited to just two stages of filtering. Instead, each PSD can be followed by upto 4 filters, giving us roll-offs ranging from 6dB/Octave to 24dB/Octave. The filter has a adjustable roll-off, and an adjustable time constant. The time constant of the filter is just  $\frac{1}{2\pi f}$  where  $f$  is the  $-3\text{dB}$  frequency. The time constants range from  $1\mu\text{s}$  to  $300\text{s}$ .

### 1.3.3. Synchronous Filters

Recall that the output of our PSD originally gave us a DC signal, and a signal at twice the detection frequency. If our detection frequency (say  $f$ ) is too small, then the  $2f$  frequency might be harder to filter out. The lower  $2f$  gets, the higher we must set the time constant and roll-off of our low pass filter. However, SR830 has synchronous filtering. The synchronous filter averages the PSD output over a period of the reference signal. Which means, all the harmonics of the detection frequency  $f$  are notched out. If our signal was perfectly clean, even the need for the Low Pass Filtering stage is removed. We only use the synchronous filter for detection frequencies under 200 Hz. Above that, removing the  $2f$  frequency using normal filter stages is feasible.

## 1.4. Noise Sources of the SR830

There are a variety of ways we can see noise in our lock-in measurements, both intrinsic (random) noise, and external noise. Below we list some of these sources in brief detail.

### 1.4.1. Johnson Noise

Due to thermal fluctuations, any resistor generates some noise across its terminals. The open circuit noise voltage for a resistor with resistance R and temperature T is given by,

$$V_{\text{noise}}(\text{rms}) = \sqrt{4K_B T R \Delta f} \quad (1.5)$$

Where  $\Delta f$  is the bandwidth of the measurement. In a lock-in, the ENBW (Equivalent Noise Bandwidth) of the low pass filters sets the measurement bandwidth. So we have,

$$V_{\text{noise}}(\text{rms}) = 0.13\sqrt{R}\sqrt{\text{ENBW}}nV \quad (1.6)$$

This ENBW is determined by the roll-off slope and the time constant of the low pass filter.

### 1.4.2. Shot Noise

Electric current has noise due to the finite nature of the charge carriers, which results in a non-uniformity in the electron flow. This noise is called shot noise. The shot noise is given by,

$$I_{\text{noise}}(\text{rms}) = \sqrt{2eI\Delta f} \quad (1.7)$$

### 1.4.3. 1/f Noise

Apart from Johnson Noise, resistors can also generate noise due to fluctuations in resistance due to the current flowing through it. Note that this noise is not thermal in nature and, has a  $\frac{1}{f}$  power spectrum. This makes measurements at low frequencies more difficult.

### 1.4.4. External Noises

Also there several external noise sources possible which have been listed below,

- Capacitive Coupling
- Inductive Coupling
- Ground Loops

## 2. Flicker Noise

After the invention of the “thermionic tube” amplifiers in 1921, C.A. Hartmann attempted an experiment to verify Schottky’s formula for the shot noise spectral density [1]; Hartmann failed, and it was J. B. Johnson (of Johnson-Nyquist fame) who measured the white noise spectrum. However, Johnson also measured an unexpected “flicker noise” at low frequencies. This is shown in the following diagram:

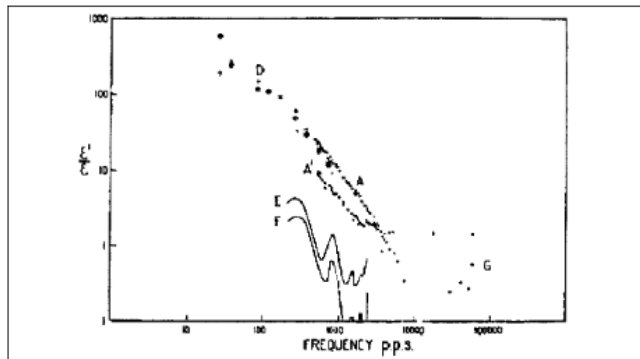


Fig. 6. Frequency variation for tube No. 2, coated filament; same data as in Fig. 4 plotted to a frequency scale; curves E and F give Hartmann's results for 2 m.a. and 20 m.a.; points G were obtained with less steady measuring circuit.

Figure 1: the spectral density observed by J. B. Johnson, as shown in his original paper [3]. The vertical scale represents the observed noise power density divided by the theoretical shot noise power density; the horizontal scale is the frequency in Hz.

**Figure 4:** (Source: [2])

It was soon found that such “flicker noise” is found in many systems. The observed spectral density of flicker noise is quite variable, as it behaves like  $\frac{1}{f^\alpha}$ , where  $\alpha \in [0.5, 1.5]$ , and this behaviour extends over several frequency decades.

The appearance of power laws in the theory of critical phenomena, and the work of B. Mandelbrot on fractals [3]; seemed to indicate something universal with noise of this spectral signature.

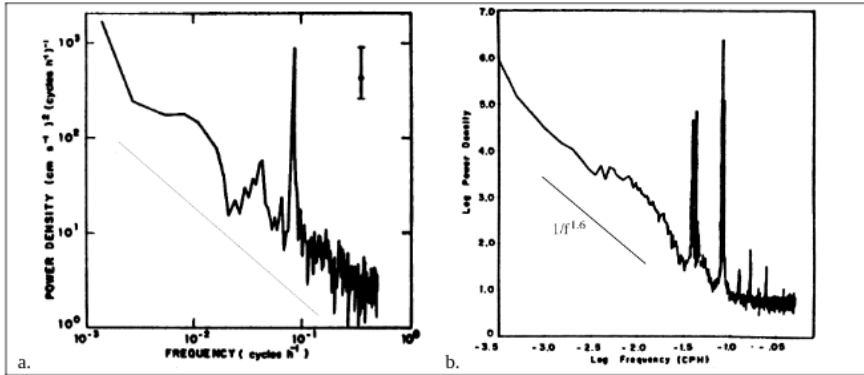


Figure 2: a. power spectrum of the east-west component of ocean current velocity [7]; the straight line shows the slope of a  $1/f$  spectrum. b. sea level at Bermuda: this is  $1/f^\alpha$  spectrum with  $\alpha \approx 1.6$  [8].

**Figure 5:** (Source: [2]; Some examples of  $1/f$  noise)

## 2.1. $\frac{1}{f^\alpha}$ noise from the superposition of relaxation processes

Some of the early explanations of the appearance of  $\frac{1}{f^\alpha}$  noise in vacuum tubes due to Johnson [4]; and Schottky [5]; aligned along these lines: There is a contribution to the vacuum tube current from the cathode surface trapping sites, which release electrons according to a simple exponential relaxation law:

$$N(t) = N_0 e^{-\lambda t}, t \geq 0 \quad (2.1)$$

The Fourier transform of a single exponential relaxation process is given by:

$$F(\omega) = \int_{-\infty}^{\infty} N(t)e^{-i\omega t} dt = N_0 \int_0^{\infty} e^{-(\lambda+i\omega)t} dt = \frac{N_0}{\lambda + i\omega} \quad (2.2)$$

If we image a sequence of such pulses, given by:

$$N(t, t_k) = N_0 e^{-\lambda(t-t_k)}, t \geq t_k \quad (2.3)$$

where  $N(t, t_k) = 0$  for  $t < t_k$ . Taking the Fourier transform of this,

$$F(\omega) = \int_{-\infty}^{\infty} \sum_k N(t, t_k) e^{-i\omega t} dt = \frac{N_0}{\lambda + i\omega} \sum_k e^{i\omega t_k} \quad (2.4)$$

Which represents a spectrum given by:

$$S(\omega) = \lim_{T \rightarrow \infty} \frac{1}{T} \langle |F(\omega)|^2 \rangle = \frac{N_0^2}{\lambda^2 + \omega^2} \lim_{T \rightarrow \infty} \frac{1}{T} \langle \left| \sum_k e^{i\omega t_k} \right|^2 \rangle = \frac{N_0^2 n}{\lambda^2 + \omega^2} \quad (2.5)$$

Where  $n$  is the average pulse rate, and the average indicated is the ensemble average. This spectrum is nearly flat at small frequencies, and after a transition region it becomes proportional to  $\frac{1}{\omega^2}$  at high frequencies. This does happen at high frequencies, and is often called “red noise”. But it does not explain the data collected by Johnson, i.e. the  $1/f$  noise.

As a next step, we can consider a superposition of such relaxation processes with a distribution of relaxation rates [6]  $\lambda$ . Let us assume that this distribution is uniform in the range  $\lambda \in [\lambda_1, \lambda_2]$ , and that the amplitude of each pulse remains the same. With this, we can derive a spectrum:

$$S(\omega) = \frac{1}{\lambda_1 - \lambda_2} \int_{\lambda_1}^{\lambda_2} \frac{N_0^2 n}{\lambda^2 + \omega^2} d\lambda = \frac{N_0^2 n}{\omega(\lambda_2 - \lambda_1)} \left[ \arctan\left(\frac{\lambda_2}{\omega}\right) - \arctan\left(\frac{\lambda_1}{\omega}\right) \right] \quad (2.6)$$

So, in different regimes, we have:

$$1. \quad S(\omega) = N_0^2 n, 0 < \omega \ll \lambda_1 \ll \lambda_2 \quad (2.7)$$

$$2. \quad S(\omega) = \frac{N_0^2 n \pi}{2\omega(\lambda_2 - \lambda_1)}, \lambda_1 \ll \omega \ll \lambda_2 \quad (2.8)$$

$$3. \quad S(\omega) = \frac{N_0^2 n}{\omega^2}, \lambda_1 \ll \lambda_2 \ll \omega \quad (2.9)$$

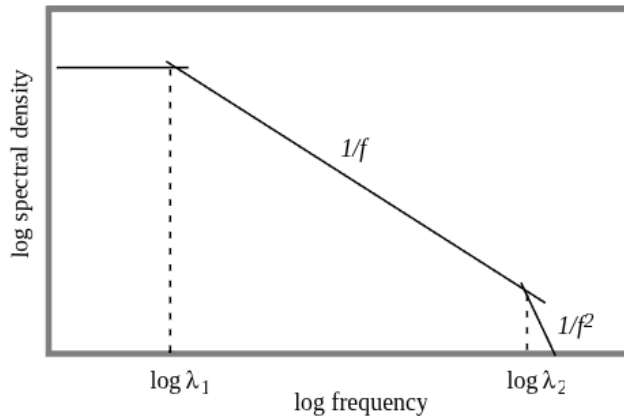


Figure 4: schematic shape of the spectral density (4). There are three characteristic regions: a white noise region at very low frequency, a  $1/f$  noise intermediate region and a  $1/f^2$  region at high frequency.

**Figure 6:** (Source: [2]; Spectrum from a uniform distribution of relaxation rates)

Numerical studies have shown that this spectrum is relatively insensitive to small deviations from a perfectly uniform distribution of relaxation rates  $\lambda$  [2].

Now, if we distribute the relaxation rates according to a distribution given by:

$$dP(\lambda) = \frac{A}{\lambda^\beta} d\lambda, \lambda \in (\lambda_1, \lambda_2) \quad (2.10)$$

we can still calculate the spectrum integral exactly, as summarised by van der Ziel [7];.. The results are:

$$S(\omega) \propto \int_{\lambda_1}^{\lambda_2} \frac{1}{\lambda^2 + \omega^2} \frac{d\lambda}{\lambda^\beta} \quad (2.11)$$

Where we get:

$$1. \quad \beta = 1 \implies S(\omega) = \frac{1}{\omega^2} \left[ \ln \left( \frac{\lambda}{\sqrt{\lambda^2 + \omega^2}} \right) \right]_{\lambda_1}^{\lambda_2} \quad (2.12)$$

$$2. \quad \beta \neq 1 \implies S(\omega) = \frac{\lambda^{1-\beta}}{(1-\beta)\omega^2} F \left[ \left( \frac{1-\beta}{2}, 1, \frac{1-\beta}{2}, -\frac{\lambda^2}{\omega^2} \right) \right]_{\lambda_1}^{\lambda_2} \quad (2.13)$$

Here,

$$F(a, b, c, d) = \frac{\Gamma(c)}{\Gamma(b)\Gamma(c-b)} \int_0^1 t^{b-1} (1-t)^{c-b-1} (1-td)^{-a} dt \quad (2.14)$$

Which is a hypergeometric function. We do not have to use the exact expression for the spectrum, as it is possible to approximate in the region  $\lambda \in (\lambda_1, \lambda_2)$  as:

$$S(\omega) \propto \int_{\lambda_1}^{\lambda_2} \frac{1}{\lambda^2 + \omega^2} \frac{d\lambda}{\lambda^\beta} = \frac{1}{\omega^{1+\beta}} \int_{\lambda_1}^{\lambda_2} \frac{1}{1 + \frac{\lambda^2}{\omega^2}} \frac{d\frac{\lambda}{\omega}}{(\frac{\lambda}{\omega})^\beta} = \frac{1}{\omega^{1+\beta}} \int_{\lambda_1/\omega}^{\lambda_2/\omega} \frac{1}{1+x^2} \frac{dx}{x^\beta} \quad (2.15)$$

Which may be simplified to:

$$S(\omega) \propto \frac{1}{\omega^{1+\beta}} \int_0^\infty \frac{1}{1+x^2} \frac{dx}{x^\beta} \propto \frac{1}{\omega^{1+\beta}} \quad (2.16)$$

Which is the  $\frac{1}{f^\alpha}$  spectra that we expected.

## 2.2. Can the fluctuations be infinitely large?

In most systems, it is seen that the  $1/f$  behaviour continues for many decades in frequency - making it impossible to determine  $\lambda_1$  and  $\lambda_2$ . Data from Pellegrini et. al shows this for voltage fluctuations in thin film resistors, where the behaviour is observed over 6 frequency decades. [8]; But this is a problem, as if this behaviour continues down to zero frequency we would have infinite integrated fluctuation as shown by:

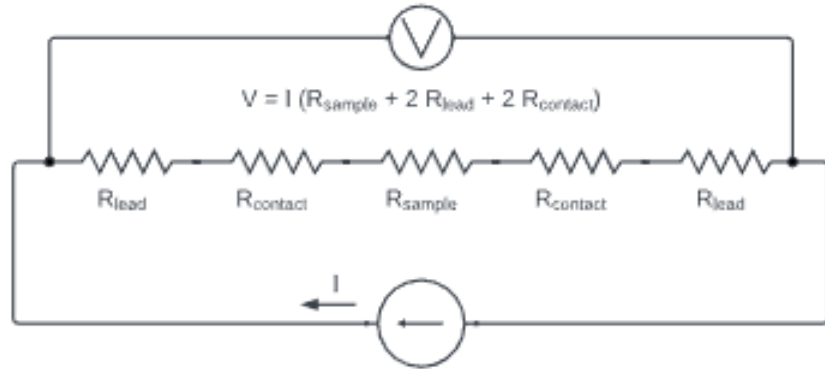
$$\int_0^\infty S(f) df \propto \lim_{f_1 \rightarrow 0, f_2 \rightarrow \infty} \int_{f_1}^{f_2} \frac{1}{f} df = \lim_{f_1 \rightarrow 0, f_2 \rightarrow \infty} \ln \frac{f_2}{f_1} \quad (2.17)$$

Which obviously diverges. This is also true for any  $\frac{1}{f^\alpha}$  spectra. Flinn [9]; produced a simple argument that shows that such a blow-up is not physical and there is no need to worry about it. Note that the integrated fluctuation for  $1/f$  noise is always the same for every frequency decade. Now, the lowest observable frequency in the universe is the inverse of the lifetime of the Universe, which is approximately  $10^{-17} Hz$ . On the other hand, if we take the Planck time as the smallest observable time, we get a frequency of approximately  $10^{43} Hz$ . So, there are a total of 59 frequency decades that are observable, which means that the highest total possible fluctuation can only be 59 times the total fluctuation between  $1Hz$  and  $10Hz$ .

## 3. Four Terminal AC Resistance Measurement

Electrical resistivity is a fundamental material property and is crucial for understanding electronic behaviour in a material. The simplest electrical resistance measurement is a 2 terminal DC measurement of voltage due to an applied current. This method is prone to noise because: 1. The system is

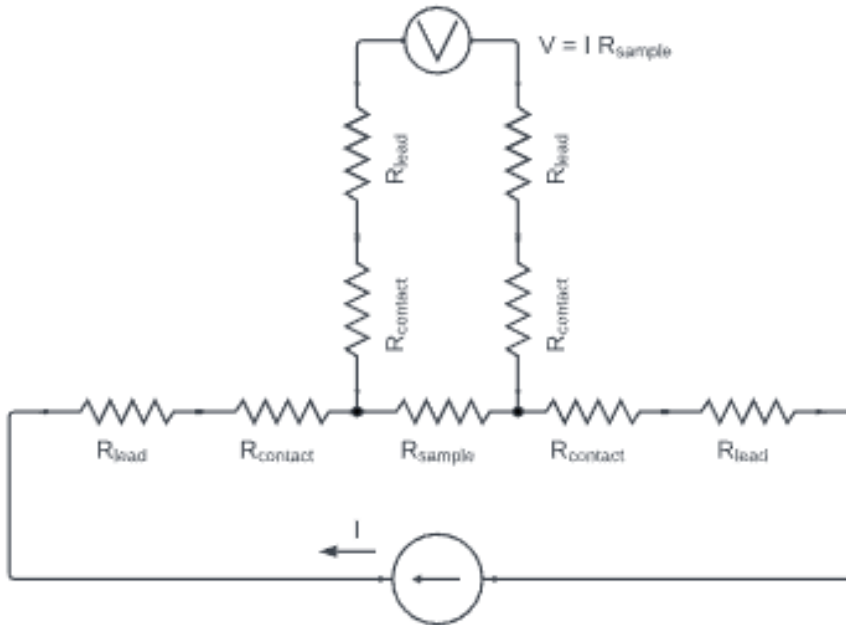
being driven at low frequency, and thus a substantial amount of  $1/f$  noise is introduced. 2. Lead and contact resistance 3. Thermal offsets



**(a)** Two-point resistance measurement, showing contributions from contacts and leads to the voltage measurement.

Figure 7: (Source: [10])

Here, we discuss the four-terminal AC resistance measurement as an alternative to the simple two-probe DC measurement.



**(b)** Four-point resistance measurement. For a high impedance voltmeter, the contact and lead resistances can be neglected.

Figure 8: (Source: [10])

There are two main advantages of the four-point AC method over the more rudimentary two-probe method - 1. The four-point geometry removes the effects of contact resistance, allowing a measurement of the intrinsic device resistance. 2. The measurement of an AC voltage at a fixed frequency of excitation current allows the use of Lock-In measurement, which provides an effective narrow

bandwidth extraction of the signal. This reduces the noise in the measurement greatly. Moreover, the measurement using AC provides some isolation from the thermoelectric voltages present in the DC measurements.

### 3.1. Contact resistance

When two metal surfaces touch, they normally do not make contact across the entire macroscopic contact surface area ( $A_m$ ). Instead, they touch only at microscopic high points on the surfaces called **asperities**. The sum of all the contact areas from the asperities is called the real contact surface area ( $A_r$ ). Normally,  $A_r \ll A_m$ . The current lines must squeeze together to pass through the asperities, and this is the primary reason for the creation of contact resistance and is called the “Constriction Resistance”. There are two main regimes involved in modelling how the asperities affect contact resistance, and they are determined by comparing the radius of the spot of asperities contact ( $a$ ) and the electron mean free path length ( $l$ ). 1. Diffusive regime ( $a \gg l$ ): Here, the electrons will scatter several times as they pass through the contact. Thus, the transport is diffusive and is governed by the Maxwell equations. The resistance contribution in this case is given by  $R_{diffusive} = \frac{\rho}{2a}$ . 2. Ballistic regime ( $a \ll l$ ): Here, the electrons travel through the contact spot without scattering. Thus, the resistance is no longer due to the scattering but rather due to the number of quantum channels available for the electron wavefunction to transmit. This is Sharvin resistance, and is derived from semiclassical transport theory to be  $R_{ballistic} = \frac{4\rho l}{3\pi a^2}$ . Normally, metal-metal contact resistance is ohmic. But due to the massive constriction of current to the asperities, there is a large current density present there. This leads to a significant amount of Joule heating. Also of interest is the fact that thermal fluctuation can result in fluctuations in  $A_r$  - which can cause a fluctuation in the effective resistance of the device seen. This is a potential source of 1/f noise in the system. Considering all these effects, it is crucial to measure the submilliohm resistance using a 4-point method as otherwise we would be measuring the contact and not the device resistance itself.

### 3.2. Preparation of sample for 4-point measurement

Note that minimising the contact resistance is good practice even in the case of 4-point measurements, as contact resistance can result in ohmic heating of the sample and introduce noise.

Ideally, contacts should be cleaned properly before making connections. Even with silver conductive paint at contact junction, contact resistances can be as large as  $10\Omega$ .

### 3.3. BNC Cables

The Bayonet Neill-Concelmann (BNC) cable is a coaxial RF cable that is designed for use in scientific data collection. The dimensions and material of the BNC cables are designed to provide a characteristic impedance to the signal. This reduces the phenomena of signal reflection at the connection point. The coaxial design of the cable acts as a Faraday cage, essentially shielding the inner wire from external electromagnetic interference. Normally, an important aspect of using BNC cables to relay a signal is **impedance matching**. When a signal is relayed down a BNC cable and it reaches the device/load, the signal can either be absorbed by the load or it can be reflected back the wire. The behaviour is quantified by the reflection coefficient, defined as:

$$\Gamma = \frac{Z_L - Z_0}{Z_L + Z_0} \quad (3.1)$$

Where  $Z_L$  is the load impedance, and  $Z_0$  is the cable impedance (usually specified very accurately). Ideally, we would want  $\Gamma = 0$ , which requires  $Z_L = Z_0$ , which is the impedance matching criteria. If we have  $\Gamma \neq 0$ , we end up having standing waves and jitters in the cable, which obviously affect measurements significantly. When is matching required? The effects of impedance mismatch become apparent only when the cable acts like a transmission line. This happens when the cable length is significant compared to the signal's wavelength. A rule of thumb is that matching is required when we have:

$$\text{Cable length} > \frac{\text{Wavelength}}{10} \quad (3.2)$$

In our case, we use driving frequencies upto  $\approx 100\text{kHz}$ . This corresponds to a wavelength of  $\approx 300m$ , and a threshold (from the rule of thumb) of  $30m$ . Since the cables we use are significantly shorter, impedance matching is not something that we concern ourselves with here. ## Setting up instrument It is to be noted that in our experiment we did not have access to a modulated constant current source that could generate a clock synchronisation signal compatible with the Lock-In Amplifier provided. Thus, we resorted to using the Lock-In Amplifier's internal reference signal to drive a modulated current through the device being measured. The drive frequency influences the measurement in many ways. A larger driving frequency may avoid significant  $1/f$  noise and allow the measurement of faster phenomena (with reasonable time constants), but it can lead to larger phase lag between the reference and the signal which may obscure the intrinsic device resistance and reduce the signal to noise ratio of the measurement as more current is shunted through the stray load capacitance. With a sample resistance  $R$  and a stray capacitance  $C$  measured at some frequency  $f$ , we will observe a phase shift of the order:

$$\theta = 2\pi fRC \quad (3.3)$$

## 4. Sub-Milliohm Resistance Measurement

In this experiment, we aim to measure the sub-milliohm resistance of a copper wire using an SR830 Lock-in Amplifier, using the four-probe method to minimize contact resistance effects. This experiment was proposed in its two probe configuration in [11]. We extend this to a four-probe configuration for better accuracy.

### 4.1. Procedure

1. Connect the copper wire sample in a four-probe configuration to the SR830 Lock-in Amplifier.
2. Our lock-in amplifier's was inconsistent in using an external current source using **REF IN**. It failed to use the external trigger of the signal generator. So we shall, instead use the signal generated by the **SINE OUT** of the lock-in amplifier itself to drive current through the sample.
3. The circuit used in given below in Figure 9, using voltage divider, we obtain the resistance of the wire  $R_w$ .
4. We set the amplitude of the lock-in amplifier to some reference value, say 2.5 V for our case.
5. We set the time constant of the lock-in amplifier and the sensitivity appropriately to get a stable reading.
6. We **AUTO PHASE** and **AUTO GAIN** the lock-in amplifier to optimize the phase and gain settings, such that the gain does
7. We record the measurements using a GPIB cable and python scripts using the **pyvisa** library.
8. We vary the frequency of the lock-in amplifier from 10 Hz to 100 kHz, and record the voltage across the inner probes.
9. For each frequency, after setting the frequency, we wait for several time constants and then record the voltage reading and the voltage fluctuations.
10. The Plots are then taken and analyzed.

## 4.2. Circuit Diagram

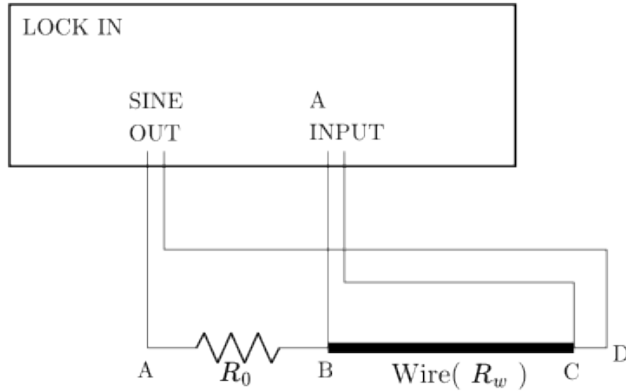


**Figure 9:** Circuit diagram for four-probe resistance measurement using SR830 Lock-in Amplifier.

The Four probe configuration uses the **SINE OUT** of the lock-in amplifier to drive current through the outer probes A and D. The voltage across the inner probes B and C is measured using the differential input of the lock-in amplifier. We now infer wire resistance  $R_w$  using the voltage divider formula. The current  $I$  through the wire is given by:

$$I = \frac{V_A - V_C}{R_0 + R_w} = \frac{V_B - V_C}{R_w} \quad (4.1)$$

Also note that  $V_C = 0$ , since it is the ground reference for the lock-in amplifier. Using this, we can derive the expression for  $R_w$  as:

$$\begin{aligned} \frac{V_A - V_C}{R_0 + R_w} &= \frac{V_B - V_C}{R_w} \\ \Rightarrow R_w &= \frac{V_B}{V_A} \frac{R_0}{1 + \frac{R_w}{R_0}} \\ \Rightarrow R_w &\approx \frac{V_B}{V_A} R_0 \text{ (since } R_w \ll R_0\text{)} \end{aligned} \quad (4.2)$$

For our experiment, we choose  $R_0 = 1kHz$ , which is much larger than the expected resistance of the copper wire, which is in the sub-milliohm range. This approximation is correct upto and order of  $10^{-6}\Omega$ .

## 4.3. Parameters

The parameters used in the experiment are tabulated below:

1. Reference Voltage Amplitude: 2.5 V
2. Reference Frequency: 10 Hz to 100 kHz (varied)
3. Series Resistor  $R_0$ : 1kΩ
4. Time Constant: 1 s
5. Sensitivity: 24 dB/oct

## 4.4. Analysis

The recorded voltage across the inner probes is used to calculate the resistance of the copper wire using the derived formula. The resistance values are plotted against the frequency to observe any frequency dependence. We collected 4 datasets. Note that we have plotted the voltages of  $R, X, Y$  from with the frequency in the log scale.

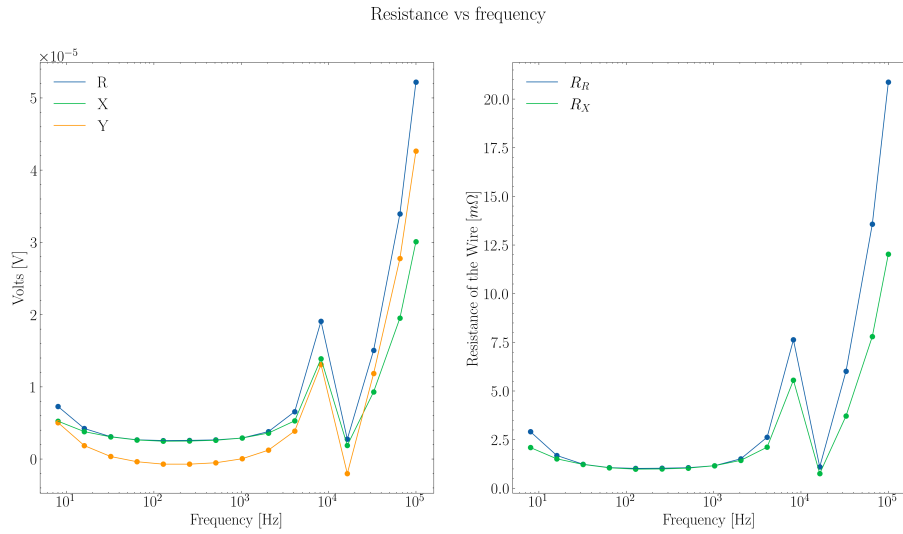


**Figure 10:** Voltage vs Frequency plot.

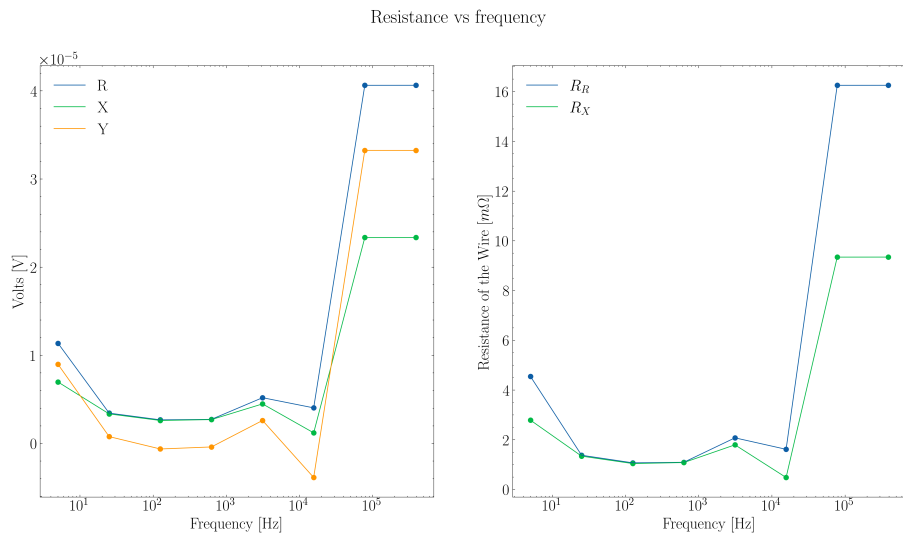


**Figure 11:** Voltage vs Frequency plot.

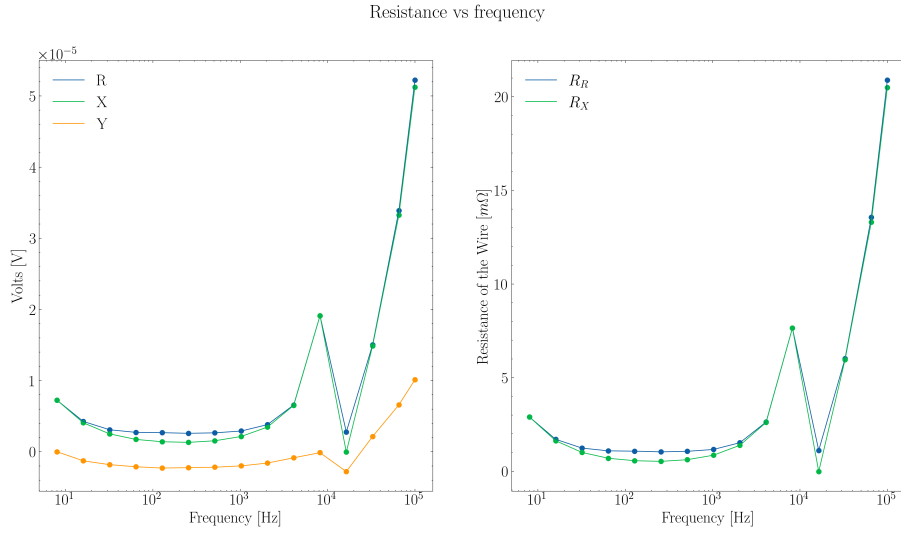


**Figure 12:** Voltage vs Frequency plot.

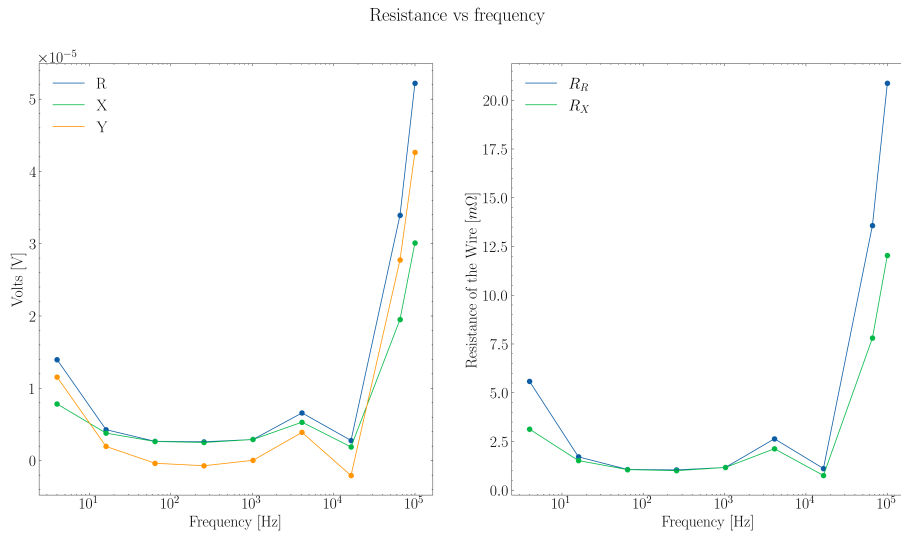


**Figure 13:** Voltage vs Frequency plot.

## 4.5. Resistance

From our datasets we take a weighed mean of the resistance values calculated from the voltage measurements in the domain of low error in around the 100 Hz range. The weighed mean resistance value is given by:

$$R_w = \frac{\sum_i \sigma_R^2 R_i}{\sum_i \sigma_R^2} \quad (4.3)$$

The error in the resistance is given by:

$$\sigma_{R_w} = \sqrt{\sum_i \sigma_R^2} \quad (4.4)$$

The resistance value of the copper wire is given as,

$$R_w = 0.27 \pm 0.071 m\Omega \quad (4.5)$$

Using the X component of the voltage, we get a similar value of resistance,

$$R_w^X = 0.23 \pm 0.087 m\Omega \quad (4.6)$$

## 4.6. Errors

The voltage plots have been calculated with error bars, which are derived from the voltage fluctuations recorded during the experiment. The error bars have been scaled by a factor of 100 for better visibility in the plots.

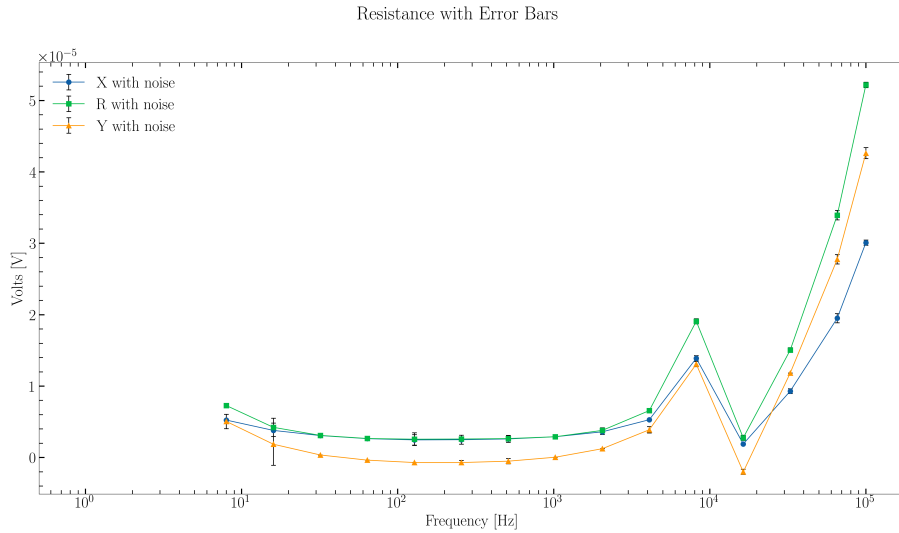


**Figure 14:** Voltage vs Frequency plot with errorbars.

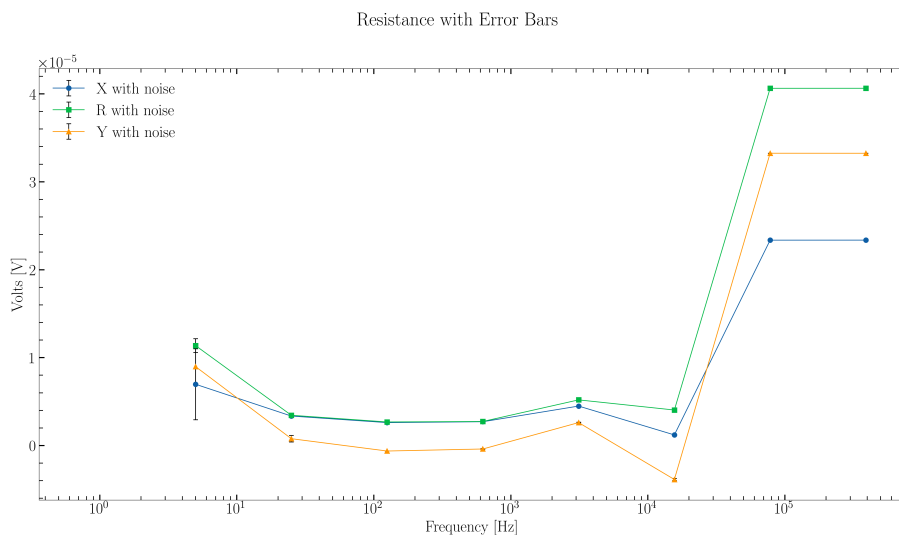


**Figure 15:** Voltage vs Frequency plot with errorbars.

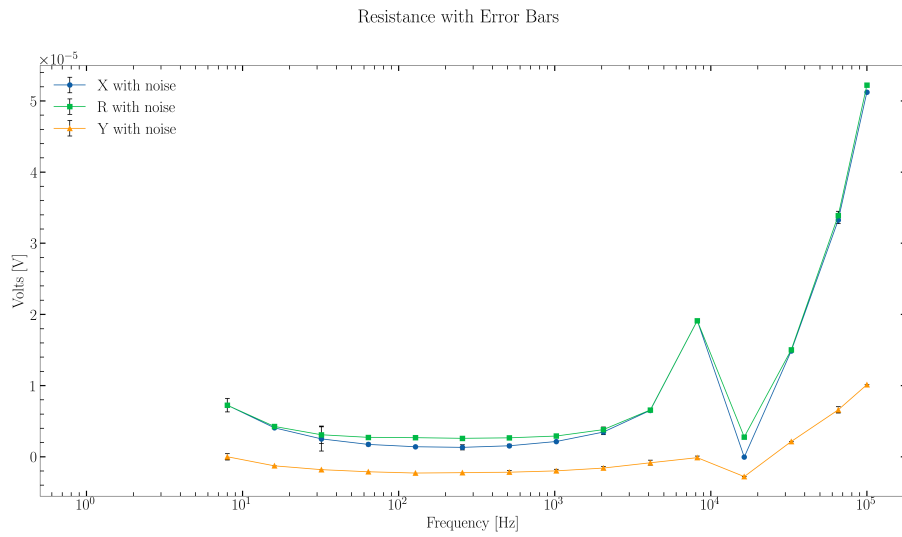


**Figure 16:** Voltage vs Frequency plot with errorbars.

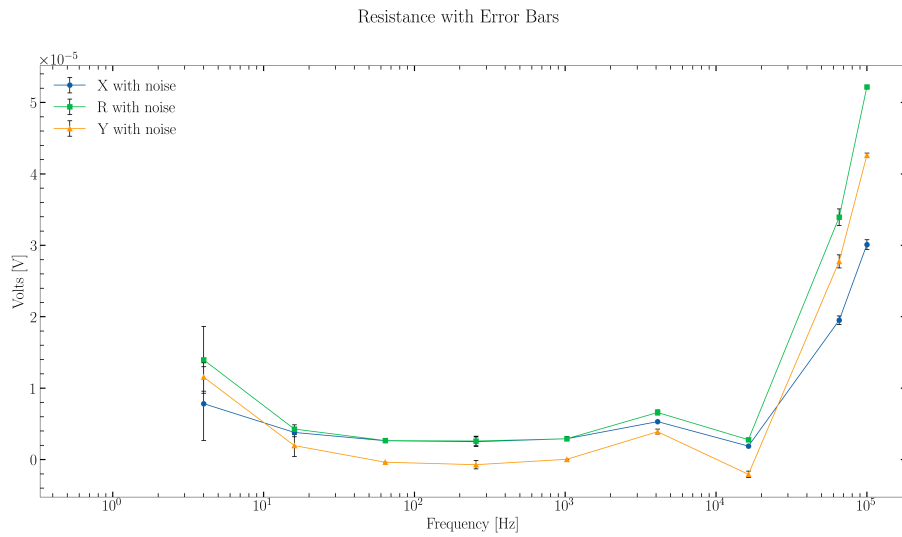


**Figure 17:** Voltage vs Frequency plot with errorbars.

## 4.7. Observations

The resistance values calculated from the voltage measurements are in the sub-milliohm range, as expected for a copper wire. Nevertheless there are some features of the graphs that are interesting.

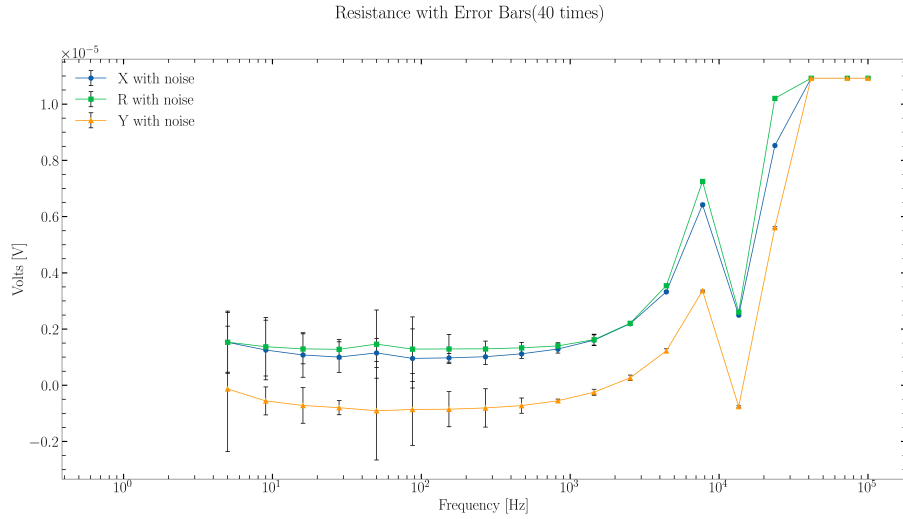


**Figure 18:** Voltage vs Frequency plot with errorbars.

Consider the graph above. At the 50 Hz frequency, we see a spike in voltage, along with a spike in voltage fluctuations. This is likely due to the power line interference at 50 Hz, since AC power lines operate at this frequency. The interference can introduce noise into the measurements, leading to increased voltage readings and fluctuations.

A much more interesting feature is the dip in voltage at around 10 kHz. This feature is present in all the datasets, albeit at slightly different frequencies. We name this unexpected effect “The Bermuda Bandwidth”. This effect is unexpected, and we do not have a clear explanation for it. The dips can be observed in all voltage components  $R, X, Y, \theta$ .

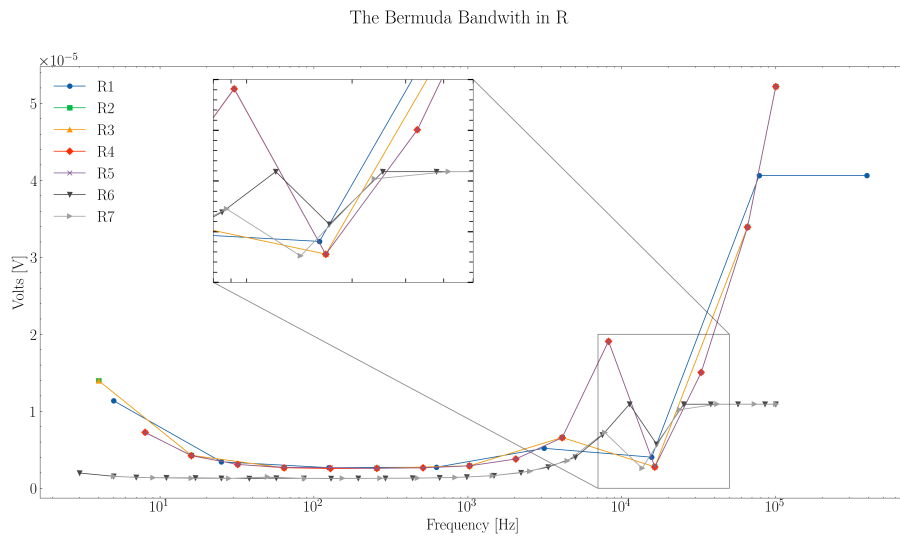


**Figure 19:** Voltage vs Frequency plot showing the dip.

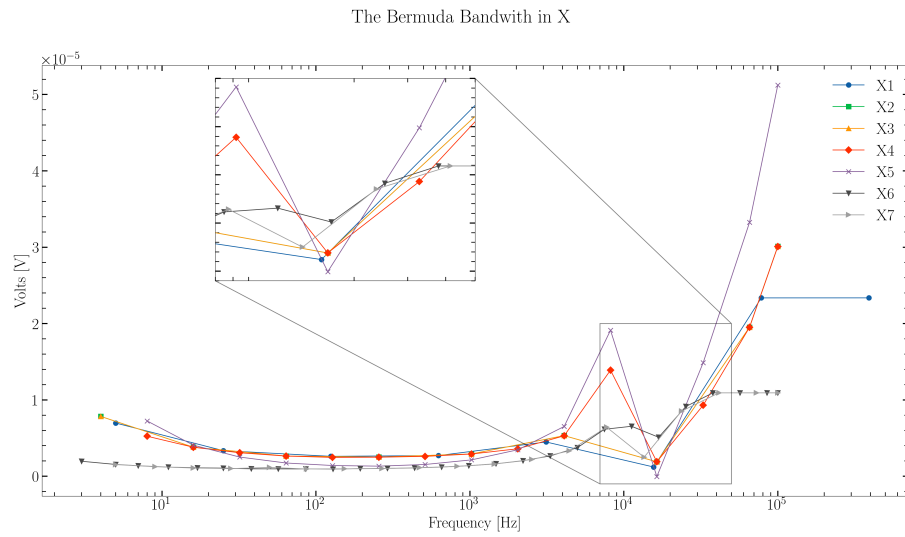


**Figure 20:** Voltage vs Frequency plot showing the dip.

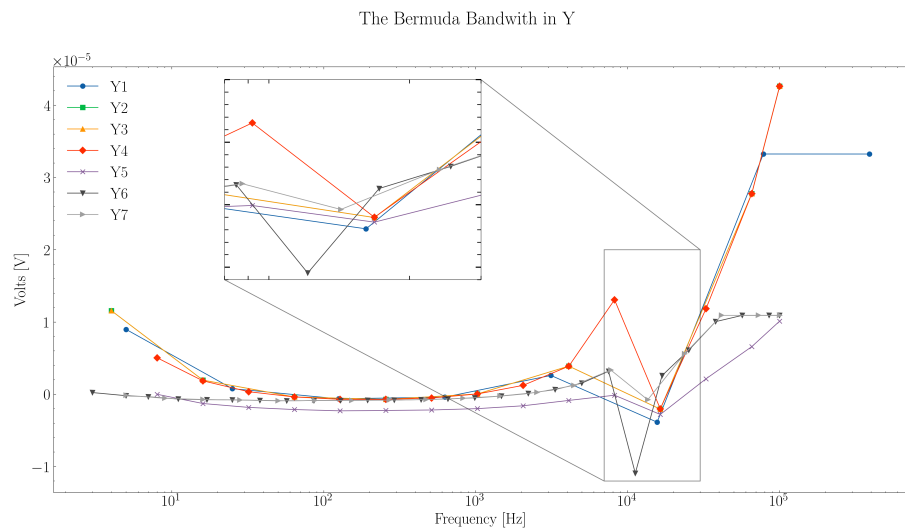


**Figure 21:** Voltage vs Frequency plot showing the dip.

The effect is however most pronounced in the phase angle theta plot.

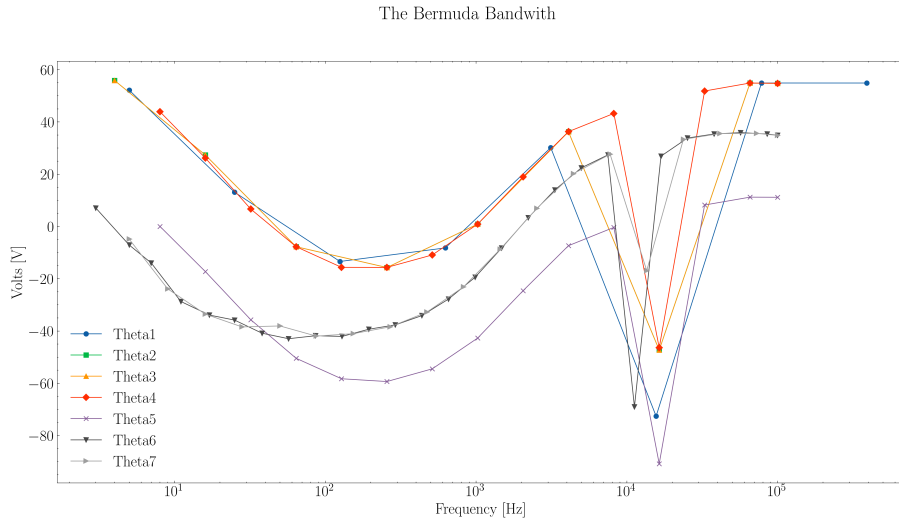


**Figure 22:** Voltage vs Frequency plot showing the dip.

At higher frequencies, above 10 kHz, the resistances blow up. This is likely due to the skin effect on conductors. As frequency increases, the alternating current creates a magnetic field that induces eddy currents within the conductor. These eddy currents are stronger near the center of the conductor and thus allow currents only on the surface of the conductor. This effectively reduces the cross-sectional area available for current flow, leading to an increase in resistance.

## 4.8. Sources of Error

The main sources of error in this experiment have been listed above in the theory section. Some other sources of error for this experiment are:

1. Capacitance and Inductance effects: At higher frequencies, the capacitance and inductance of the wires and contacts can introduce additional impedance, affecting the voltage measurements.
2. The Lock-in used by us had an inconsistent behaviour when using an external current source. This led us to use the internal signal generator of the lock-in itself, which may have introduced additional errors.
3. The BNC cable connection to the Lockin amplifier may have introduced additional noise and errors in the measurements.
4. Frequency measurements done near 50Hz harmonics may have been affected by power line interference. We have seen an example of that in our data.

## 4.9. Conclusion

In this experiment, we successfully measured the sub-milliohm resistance of a copper wire using a four-probe configuration with an SR830 Lock-in Amplifier. The results indicate that the resistance values are in the expected range.

One hint about the next part of our report can be gleaned from the fact that the errorbars are larger in the lower frequency domain, which leads to our next section on  $\frac{1}{f}$  noise analysis.

## 5. 1/f noise analysis

In this section, we analyze the voltage fluctuations recorded during the resistance measurements to investigate the presence of  $\frac{1}{f}$  noise, also known as flicker noise. This type of noise is characterized by a power spectral density that is inversely proportional to the frequency, and it is commonly observed in electronic devices and materials.

In resistors, we model this noise using the relaxation model derived in the theory section. Resistors have defects that can trap and release charge carriers, leading to fluctuations in resistance and voltage, which cause the observed  $\frac{1}{f}$  noise.

## 5.1. Working Principle

Generally,  $\frac{1}{f}$  noise can be characterised by its power spectral density (PSD), which is obtained from the Fourier transform of the autocorrelation function of the voltage signal. However for a lockin amplifier, the voltage fluctuations die down rapidly due to the filtering with specifications mentioned in the manual. Therefore, we directly analyze the variance of the voltage signal as a function of frequency to identify the presence of  $\frac{1}{f}$  noise. To do that, we must analyse why that works and how erroneous it is.

Let the noise be denoted by the variable  $x(t)$ . The power spectral density  $S(f)$  is defined as:

$$S(f) = \lim_{T \rightarrow \infty} \frac{1}{T} |\hat{x}_T(f)|^2 \quad (5.1)$$

where  $\hat{x}_T(f)$  is the Fourier transform of the signal  $x(t)$  over a time interval  $T$ . The average power in a frequency band  $[f_1, f_2]$  is then given by:

$$\langle P \rangle \propto \int_{f_1}^{f_2} S(f) df \quad (5.2)$$

We assume that the lock-in does not have an ideal rectangular filter, but rather a band-pass filter with a finite bandwidth  $\Delta f$  around the reference frequency  $f$ . Then we can relate the average voltage fluctuations in the bandwidth  $[f, f + \Delta f]$  to the power spectral density. The average power in this band is:

$$\langle P \rangle_f \propto \int_f^{f+\Delta f} S(f) df \quad (5.3)$$

If we assume that the noise follows a  $\frac{1}{f}$  dependence, i.e.  $S(f) = \frac{A}{f}$ , where  $A$  is a constant, Assuming that  $\Delta f$  is small compared to  $f$ , we can approximate the integral as:

$$\langle P \rangle_f \propto \frac{A}{f^2} \Delta f \quad (5.4)$$

Note that  $P$  here is the power of the noise signal. One assumption here is that the noise voltage also follows the same dependence, i.e.  $V^2 \propto P$ . Therefore, we can write:

$$\langle V_{\text{noise}}^2 \rangle_f \propto \frac{1}{f^2} \quad (5.5)$$

Note for our case, the signal is the average voltage  $\langle V \rangle$ , then the Noise voltage is given by  $V_{\text{noise}} = V - \langle V \rangle$ . We can thus see that,

$$\delta V_{\text{noise}} = \sqrt{\langle V_{\text{noise}}^2 \rangle} \propto \frac{1}{f} \quad (5.6)$$

The errors in this approximation arise as powers of  $\frac{\Delta f}{f}$ . So one way to mitigate the error due to approximation is to ignore lower values of  $f$ .

## 5.2. Parameters

The parameters used for the  $\frac{1}{f}$  noise analysis are as follows:

1. Reference Voltage Amplitude: 10 mV
2. Reference Frequency: 10 Hz to 100 kHz (varied)
3. Series Resistor  $R_0$ : 1 kΩ
4. Time Constant: 10 ms
5. Sensitivity: 6 dB/oct

The experimental procedure is the exact same as described in the previous section. Except here, we focus on recording the voltage fluctuations at each frequency setting of the lock-in amplifier.

### 5.3. Data analysis

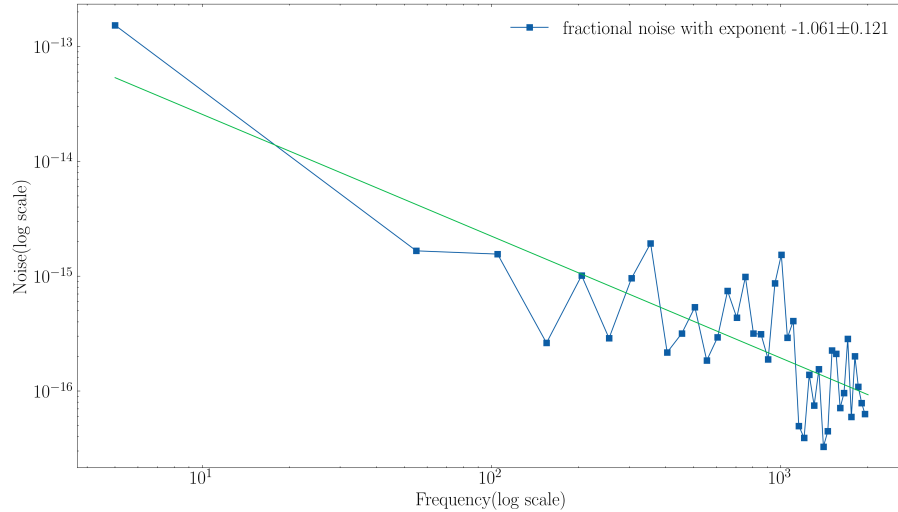


**Figure 23:** Noise Voltage vs Frequency plot with the sync filter turned on.

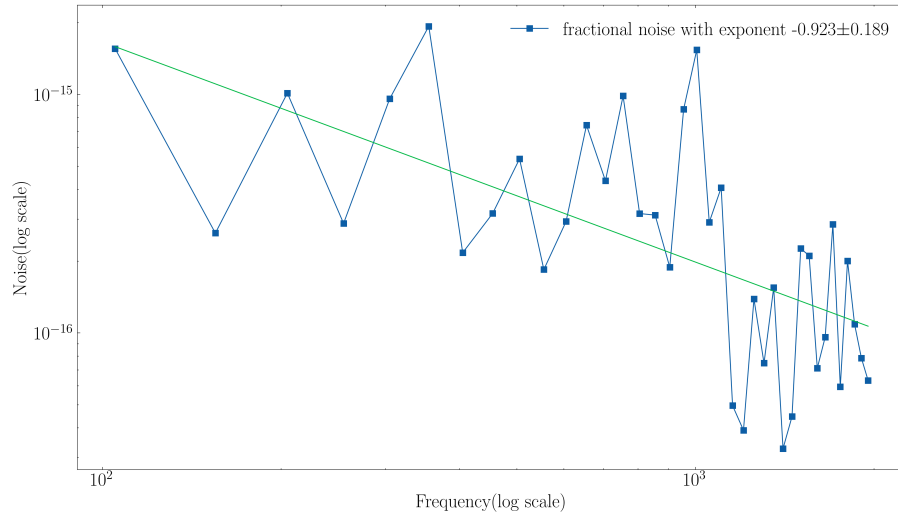


**Figure 24:** Noise Voltage vs Frequency plot with the sync filter turned on and initial datapoints removed.

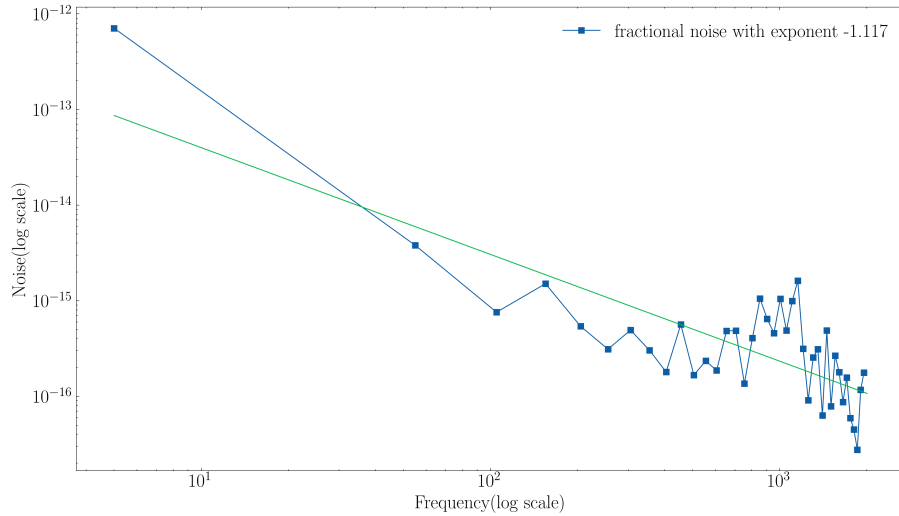


**Figure 25:** Noise Voltage vs Frequency plot with the sync filter turned off.

## 5.4. Observations

We observe  $\frac{1}{f}$  noise in the data both in datasets with the sync filter turned on and the sync filter turned off. The data with the sync filter turned on shows a clearer  $\frac{1}{f}$  dependence after removing the initial datapoints, which are likely affected by low-frequency noise and approximation errors. The data with the sync filter turned off also exhibits  $\frac{1}{f}$  behavior, but with more scatter.

## 6. Conclusion

We observed that the four-probe method using a lock-in amplifier is effective for measuring sub-milliohm resistances. The resistance of the given copper wire is measured to be ,

$$\begin{aligned} R_w &= (0.27 \pm 0.071)m\Omega \\ R_w^X &= (0.23 \pm 0.087)m\Omega \end{aligned} \tag{6.1}$$

In our analysis of the flicker noise, we found that the noise voltage follows a  $\frac{1}{f}$  dependence, both with synchronous filter on and off. The bermuda bandwidth effect observed around 10 kHz remains unexplained and warrants further investigation.

## References

- [1] C. A. Hartmann, "Über die Bestimmung des elektrischen Elementarquantums aus dem Schrotteffekt," *Annalen der Physik*, vol. 65, p. 51–?, 1921.
- [2] E. Milotti, "1/f noise: a pedagogical review." [Online]. Available: <https://arxiv.org/abs/physics/0204033>
- [3] B. B. Mandelbrot, *Fractals: Form, Chance and Dimension*. W. H. Freeman, Co., 1977.
- [4] J. B. Johnson, "The Schottky Effect in Low Frequency Circuits," *Physical Review*, vol. 26, no. 1, pp. 71–85, July 1925, doi: [10.1103/physrev.26.71](https://doi.org/10.1103/physrev.26.71).
- [5] W. Schottky, "Über spontane Stromschwankungen in verschiedenen Elektrizitätsleitern," *Physical Review*, vol. 28, no. 1, pp. 74–100, July 1926, doi: [10.1103/physrev.28.74](https://doi.org/10.1103/physrev.28.74).
- [6] J. Bernamont, "Fluctuations in the resistance of thin films," *Proceedings of the Physical Society*, vol. 49, no. 4S, pp. 138–139, Aug. 1937, doi: [10.1088/0959-5309/49/4s/316](https://doi.org/10.1088/0959-5309/49/4s/316).
- [7] A. Van Der Ziel, "Flicker Noise in Electronic Devices," in *Advances in Electronics and Electron Physics*, Elsevier, 1979, pp. 225–297. doi: [10.1016/s0065-2539\(08\)60768-4](https://doi.org/10.1016/s0065-2539(08)60768-4).
- [8] B. Pellegrini, R. Saletti, P. Terreni, and M. Prudenziati, " $\frac{1}{f^\gamma}$  noise in thick-film resistors as an effect of tunnel and thermally activated emissions, from measures versus frequency and temperature", *Physical Review B*, vol. 27, no. 2, pp. 1233–1243, Jan. 1983, doi: [10.1103/physrevb.27.1233](https://doi.org/10.1103/physrevb.27.1233).
- [9] I. FLINN, "Extent of the 1/f Noise Spectrum," *Nature*, vol. 219, no. 5161, pp. 1356–1357, Sept. 1968, doi: [10.1038/2191356a0](https://doi.org/10.1038/2191356a0).
- [10] P. M. Neves, "Four Point AC measurements." [Online]. Available: <https://www.thinksrs.com/downloads/pdfs/tpapers/four-point-resistance.pdf>
- [11] K. G. Libbrecht, E. D. Black, and C. M. Hirata, "A basic lock-in amplifier experiment for the undergraduate laboratory," *American Journal of Physics*, vol. 71, no. 11, pp. 1208–1213, Oct. 2003, doi: [10.1119/1.1579497](https://doi.org/10.1119/1.1579497).